

Incipient Fault Detection and Location in Distribution Networks: A Data-Driven Approach

Xin Shi², Robert Qiu^{1,2}, *Fellow, IEEE*, Xing He², Lei Chu², Zenan Ling²

Abstract—In this paper, a data-driven Methodology is developed for the incipient fault detection and location in distribution networks. First, the online monitoring data in the distribution network is analyzed and processed. This makes an amplification of observed sudden changes and abnormal fluctuations in data. Based on the random matrix theory for the spectrum analyzes of the spatio-temporal data matrices among multiple-time-instant monitoring devices, a real-time incipient fault detection and location algorithm is designed. During which, the linear eigenvalue statistics are defined to indicate data behavior, and the fault latencies are analyzed and located. As for those low-dimensional data matrices formed in the distribution network, by using tensor product, an increasing data dimension approach is developed to meet the prerequisites for using random matrix theory. Theoretical justifications for the algorithm is provided through Marchenko-Pastur Law and Ring Law. Case studies on the synthetic data from IEEE standard bus system and real-world online monitoring data in a power grid corroborate the feasibility and effectiveness of the proposed methodology.

Index Terms—incipient fault detection and location, distribution networks, online monitoring data, random matrix theory, tensor product

I. INTRODUCTION

THE distribution network is an important part of the power system, and its operating status is directly related to the safety of the entire system. With numerous branch lines and complicated network structure, it becomes difficult to realize early fault detection and location in the distribution network. Here, the term “early faults”, also called incipient faults, refers to certain pre-fault “symptoms” or electrical activities taking place prior to a distribution network system failure or blackout. They may present intermittent, asymmetric, and sporadic spikes, which are random in magnitude and could involve sporadic bursts as well, and exhibit complex, nonlinear, and dynamic characteristics [1]. On this occasion, model-based methods are questionable because they are usually based on certain assumptions and simplifications.

Along the years, there have been significant deployments of online monitoring systems in distribution networks. The data

This work was partly supported by N.S.F. of China No.61571296 and N.S.F. of US Grant No. CNS-1247778, No. CNS-1619250.

¹ Electrical and Computer Engineering Department, Tennessee Technological University, Cookeville, TN 38505 USA. Dr. Qiu is also with Department of Electrical Engineering, Research Center for Big Data Engineering Technology, State Energy Smart Grid Resarch and Development Center, Shanghai Jiaotong University, Shanghai 200240, China. (e-mail: rcqiu@sjtu.edu.cn)

² Department of Electrical Engineering, Research Center for Big Data Engineering Technology, State Energy Smart Grid Resarch and Development Center, Shanghai Jiaotong University, Shanghai 200240, China. (e-mail: dugushixin@gmail.com; hexing_hx@126.com; leochu@sjtu.edu.cn; ling_zenan@163.com)

collected through them contain rich information on operating status of distribution networks, which stimulates the research developments of data-driven methods. In [2], a real-time fault detection and faulted line identification functionality in active distribution networks is proposed. It merges the fault detection and location functionalities by using phasor-measurement-unit(PMU)-based state estimation. In [3], the dimensionality of the PMU data is analyzed and an online application for early event detection using the reduced dimensionality is proposed. In [4], a density-based detection algorithm is proposed to detect local outliers. It can differentiate high-quality synchrophasor data from the low-quality during system physical disturbances. In [5], by using massive streaming phasor measurement unit data, a real-time power state detection algorithm based on the multiple high dimensional covariance matrix test is developed. Feasibility of the method is validated and it can effectively reveal the attributes of a system event.

The random matrix theory (RMT), which starts in the early 20th century, is one important mathematical tool for statistical analysis of high-dimensional data. Through analyzing the statistical characteristics of the eigenvalues of target data matrices, it can reveal the regular or abnormal behavior contained in the data, thus helping exploring the complex interconnected system in macroscopical. So far, the RMT has been widely used in wireless communication [6], finance [7], quantum information [8][9], etc. However, its application in power system has just begun in recent years. In [10], an architecture with the application of the RMT into smart grids is proposed. In [11], based on the RMT, a data-driven method to reveal the correlations between factors and the power system status is proposed. In [12], [13], the RMT is used for power system transient analysis and steady-state analysis respectively.

In this paper, based on the RMT, we propose a fully data-driven methodology to realize incipient fault detection and location in distribution networks. It merges fault detection and location functionalities by using online monitoring data. For each main feeder in the distribution network, a spatio-temporal data matrix among multiple-time-instant monitoring devices is presented as data source. The data collected from each monitoring device can be three-phase voltages, three-phase currents, active power, reactive power, etc. Then, we conduct real-time analysis by using moving split-window method and the RMT, and compare their findings with the theoretical values (i.e., Marchenko-Pastur Law and Ring Law). During the period, the linear eigenvalue statistic (LES), a high-dimensional statistical magnitude for the spatio-temporal data matrix, is used to indicate the data behavior. Considering those low-dimensional data matrices formed by some main feeders,

by using tensor product, an increasing data dimension method is developed to meet the prerequisites for using the RMT. As for the judged faulted feeder, analyses of the latencies introduced by different branch lines are provided. The main features of the proposed methodology can be summarized as follows: 1) It is a fully data-driven methodology without requiring too much prior knowledge on the complex topology or parameter information of distribution networks. 2) Based on the RMT, the proposed methodology merges fault detection and location functionalities by using online monitoring data. 3) It is theoretically justified that the proposed methodology is robust against random fluctuations and measuring errors, which can reduce the potential false alarm probability. 4) Both on-line and off-line analysis can be handled in this proposed methodology. 5) The proposed methodology is capable of detecting incipient faults and locating them in real-time, which can help control those fault events at an early stage and reduce power failure times.

The rest of this paper is organized as follows. Section II presents the RMT for spectrum analyzes of random matrices under both normal and abnormal status, defines LES, and gives the detailed steps of the RMT for abnormal detection and location. In section III, spatio-temporal matrices are formed by using online monitoring data in distribution networks and specific procedures of incipient fault detection and location algorithm based on RMT are designed. As for those low-dimensional data matrices formed by some main feeders, an increasing data dimension method is developed for them to meet the prerequisites of using the RMT. Both synthetic data from IEEE standard bus system and real-world online monitoring data from a grid are used to validate the effectiveness of the proposed methodology in section IV. Conclusions and possible further research directions are presented in Section V.

II. RANDOM MATRIX THEORY FOR ABNORMAL DETECTION

The RMT was first introduced in mathematical statistics in the early 20th century. As for large random matrices, the importance of the RMT for statistics comes from the fact that it may be used to correct traditional tests or estimators which fail in the ‘large p , large t ’ setting, where p is the number of parameters (dimensions) and t is the sample size [14]. In practical world, massive data can be naturally represented by large random matrices [15]. With the arise of large dimensional data sets in various fields, the RMT has been used as an important mathematical tool for studying the statistical properties of functions of them.

A. Statistical Properties of Normal and Abnormal Random Matrices

Let \mathbf{X} be a $p \times t$ random matrix. According to the RMT, when $p, t \rightarrow \infty$ but $\frac{p}{t} \rightarrow c \in (0, \infty)$, the empirical spectral distribution (ESD) of its corresponding covariance matrix or the product of singular value equivalent matrix will converge to some theoretical limits, such as Marchenko-Pastur Law (MP-law) and Ring Law (Ring-law). In this subsection, by using

MP-law and Ring-law, we will discuss ESD and compare it with the theoretical values under both normal and abnormal statuses.

1) Marchenko-Pastur Law Case: Let $\mathbf{X} = \{x_{i,j}\}$ be a $p \times t$ random matrix, whose entries are independent identically distributed (i.i.d.) variables with the mean $\mu(x) = 0$ and the variance $\sigma^2(x) < \infty$. The corresponding covariance matrix is defined as $\Sigma = \frac{1}{t} \mathbf{X} \mathbf{X}^H$. As $p, t \rightarrow \infty$ but $c = \frac{p}{t} \in (0, 1]$, according to the MP-Law [16], ESD of Σ converges to the limit with probability density function (PDF)

$$f_{MP}(x) = \begin{cases} \frac{1}{2\pi c\sigma^2 x} \sqrt{(b-x)(x-a)}, & a \leq x \leq b \\ 0, & \text{others} \end{cases}, \quad (1)$$

where $a = \sigma^2(1 - \sqrt{c})^2$, $b = \sigma^2(1 + \sqrt{c})^2$.

In normal state, according to the MP-law, the ESD of the Wishart matrix Σ converges to the spectral density $f_{MP}(x)$, which is shown in Figure 1a. The bars in blue color indicate the eigenvalue distribution of Σ and the MP-law is plotted in the red curve. However, what will happen in abnormal state? Here, “abnormal” usually means signals occur in the random matrix \mathbf{X} and the correlations among its rows have been changed. Figure 1b shows the results: the empirical spectral density of the Wishart matrix Σ can not be fit by the MP-law. It can be observed that the spikes caused by the outliers are out of range.

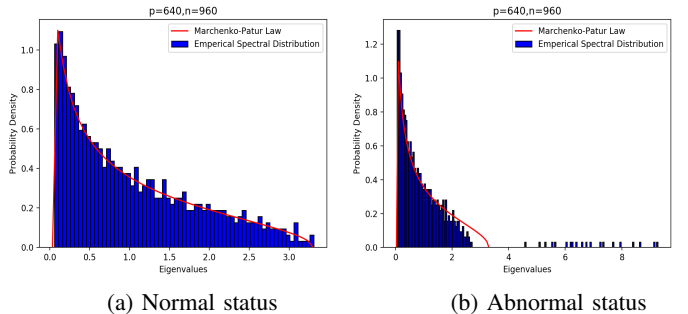


Fig. 1: ESD of Σ and its comparison with the theoretical MP-law both under normal and abnormal status.

2) Ring law Case: Assume $\mathbf{A} \in \mathbb{C}^{p \times t}$ be a non-Hermitian random matrix with i.i.d. entries $a_{i,j}$. The mean $\mu(a) = 0$ and the variance $\sigma^2(a) = 1$. The products of L non-Hermitian random matrix can be defined as

$$Z = \prod_{k=1}^L \mathbf{A}_{u,k}, \quad (2)$$

where \mathbf{A}_u is the singular value equivalent [17] of \mathbf{A} . The product \mathbf{Z} can be standardized into $\hat{\mathbf{Z}}$ (i.e., $\sigma^2(\hat{z}) = \frac{1}{p}$). As $p, t \rightarrow \infty$ but $c = \frac{p}{t} \in (0, 1]$, according to the Ring-law [18][19], the ESD of $\hat{\mathbf{Z}}$ converges to the limit with PDF

$$f_{RL}(x) = \begin{cases} \frac{1}{\pi c L} |x|^{(\frac{2}{L}-2)}, & (1-c)^{\frac{L}{2}} \leq |x| \leq 1 \\ 0, & \text{others} \end{cases}. \quad (3)$$

In normal state, we can see that the ESD of $\hat{\mathbf{Z}}$ converges to the spectral density $f_{RL}(x)$, which is shown in Figure 2a. In the complex plane, the blue dots represent the eigenvalues

of $\hat{\mathbf{Z}}$, the inner red circle radius is $(1 - c)^{\frac{L}{2}}$, and the outer red circle radius is unity. In abnormal state, the ESD of $\hat{\mathbf{Z}}$ and the Ring-law are plotted in Figure 2b. It can be observed that

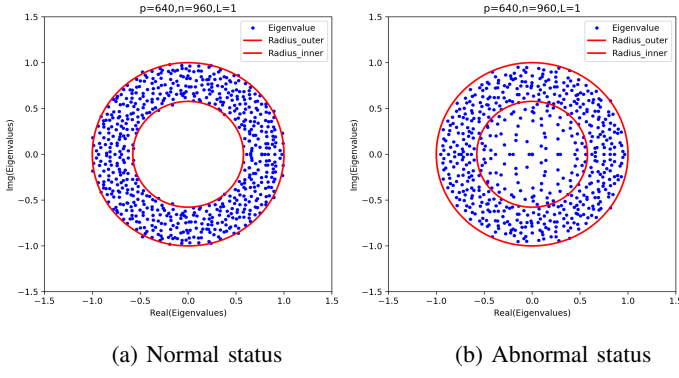


Fig. 2: ESD of $\hat{\mathbf{Z}}$ and its comparison with the theoretical Ring-law both under normal and abnormal status.

some blue dots are scattered within the radius of the inner circle. We can conclude that the ESD of $\hat{\mathbf{Z}}$ does not converge to the Ring-law.

3)Linear Eigenvalue Statistics: From the discussions of 1) and 2), it can be obtained that the eigenvalue distribution can indicate the data behavior of a large random matrix, which inspires us to find a statistic regarding eigenvalues. LES is just a high-dimensional statistical magnitude for the eigenvalues, which can be defined as [20]

$$\mathcal{N}(\phi) = \sum_{i=1}^n \phi(\lambda_i), \quad (4)$$

where $\lambda_i (i = 1, 2, \dots, n)$ are the eigenvalues, and $\phi(\cdot)$ is a test function. The commonly used test functions include

- Chebyshev Polynomial (CP): $\phi(\lambda) = a_0 \lambda^n + a_1 \lambda^{n-1} + \dots + a_n$, where $a_i (i = 1, 2, \dots, n)$ are real numbers;
- Information Entropy (IE): $\phi(\lambda) = -\lambda \log \lambda$;
- Likelihood Radio Function (LRF): $\phi(\lambda) = \lambda - \log \lambda - 1$;
- Wasserstein Distance (WD): $\phi(\lambda) = \lambda - 2\sqrt{\lambda} + 1$.

In the complex plane of Eigenvalues, the mean spectral radius (MSR), which can be regarded as a special form of LES, is used to indicate the eigenvalue distribution. It is the mean distribution radius of eigenvalues, which can be defined as

$$\kappa_{MSR} = \frac{1}{n} \sum_{i=1}^n |\lambda_i|, \quad (5)$$

where $|\lambda_i|$ is the radius of the eigenvalue λ_i on the complex plane.

B. RMT for Abnormal Detection and Location

In practice, we assume there are P -dimensional observations $(x_1, x_2, \dots, x_P) \in \mathbb{C}^P$. At the sampling time t_j , measured data of the P -dimensional observations can be formed as a column vector $\mathbf{x}(t_j) = (x_1, x_2, \dots, x_P)^H$. For a series of time T , by arranging these vectors \mathbf{x} in chronological order, we can obtain the data source \mathbf{D} for further analysis.

By using a $p \times t$ split-window on \mathbf{D} , we can obtain a raw data matrix $\mathbf{X} \in \mathbb{C}^{p \times t}$. For each matrix \mathbf{X} , we can convert it into the standard form matrix $\hat{\mathbf{X}}$ by

$$\hat{x}_{ij} = (x_{ij} - \mu(\mathbf{x}_i)) \times \frac{\sigma(\hat{\mathbf{x}}_i)}{\sigma(\mathbf{x}_i)} + \mu(\hat{\mathbf{x}}_i), \quad (6)$$

where $\mathbf{x}_i = (x_{i1}, x_{i2}, \dots, x_{it})$, $\mu(\hat{\mathbf{x}}_i) = 0$, and $\sigma(\hat{\mathbf{x}}_i) = 1$ ($i = 1, 2, \dots, p; j = 1, 2, \dots, t$). The standardization process in practice i.e. in Python, can be performed by using `sklearn.preprocessing.scale()` function.

For the standard matrix $\hat{\mathbf{X}}$, the corresponding covariance matrix is computed by

$$\Sigma = \frac{1}{T} \hat{\mathbf{X}} \hat{\mathbf{X}}^H. \quad (7)$$

Then we can compute the eigenvalues λ_{Σ} and the eigenvectors \mathbf{v}_{Σ} , which in Python, can be performed using `numpy.linalg.eig()` function. In order to characterize the distribution of the eigenvalues, the LES is defined and computed by

$$\mathcal{N}_{\Sigma}(\phi) = \sum_{i=1}^n \phi(\lambda_{\Sigma,i}), \quad (8)$$

where $\lambda_{\Sigma,i} (i = 1, 2, \dots, n)$ are the eigenvalues of Σ , and $\phi(\cdot)$ is the selected test function.

For the computed eigenvalues λ_{Σ} and eigenvectors \mathbf{v}_{Σ} of the covariance matrix $\Sigma = \{\varepsilon_{ij}\}_{p \times p}$, according to their definitions in matrix theory, we can obtain

$$\Sigma \mathbf{v}_{\Sigma,k} = \lambda_{\Sigma,k} \mathbf{v}_{\Sigma,k}. \quad (9)$$

The derivation of Equation (9) regarding the elements ε_{ij} is

$$\frac{d\Sigma}{d\varepsilon_{ij}} \mathbf{v}_{\Sigma,k} + \Sigma \frac{d\mathbf{v}_{\Sigma,k}}{d\varepsilon_{ij}} = \frac{d\lambda_{\Sigma,k}}{d\varepsilon_{ij}} \mathbf{v}_{\Sigma,k} + \lambda_{\Sigma,k} \frac{d\mathbf{v}_{\Sigma,k}}{d\varepsilon_{ij}}. \quad (10)$$

We consider the case that \mathbf{X} is real, then Σ is real and symmetric, and there exist $\mathbf{v}_{\Sigma,k}^H \mathbf{v}_{\Sigma,k} = 1$. Left multiply $\mathbf{v}_{\Sigma,k}^H$ for equation (10), we can obtain

$$\frac{d\lambda_{\Sigma,k}}{d\varepsilon_{ij}} = \mathbf{v}_{\Sigma,k}^H \frac{d\Sigma}{d\varepsilon_{ij}} \mathbf{v}_{\Sigma,k}, \quad (11)$$

where $\frac{d\Sigma}{d\varepsilon_{ij}}$ gets the value of 1 only for the element ε_{ij} in Σ and 0 for others. So equation (11) can be simplified as

$$\frac{d\lambda_{\Sigma,k}}{d\varepsilon_{ij}} = v_{\Sigma,k}^{(i)} v_{\Sigma,k}^{(j)}. \quad (12)$$

Then the contribution of the i th row's elements to $\lambda_{\Sigma,k}$ can be computed by

$$\sum_{j=1}^p \left(\frac{d\lambda_{\Sigma,k}}{d\varepsilon_{ij}} \right)^2 = (v_{\Sigma,k}^{(i)})^2 \sum_{j=1}^p (v_{\Sigma,k}^{(j)})^2 = (v_{\Sigma,k}^{(i)})^2. \quad (13)$$

From equation (13), we can conclude that the i th row's contribution to the eigenvalue $\lambda_{\Sigma,k}$ can be measured by the i th element of the corresponding eigenvector $\mathbf{v}_{\Sigma,k}$. This inspires us to realize abnormal location by studying the corresponding eigenvectors of the outliers. Here, an abnormal location indicator is designed as

$$\eta_i = \frac{\sum_{\lambda_{\Sigma,k} \in \text{outliers}} \lambda_{\Sigma,k} (v_{\Sigma,k}^{(i)})^2}{\sum \lambda_{\Sigma,k}}, \quad (14)$$

where $\eta_i \in [0, 1]$. The indicator η_i measures the scale of the i th row's induction to the abnormal. Thus we can obtain abnormal location indexes that correspond to those obviously larger values of η_i .

In real-time analysis, we can continuously obtain the raw data matrices by using a sliding-window method, i.e. moving the $p \times t$ split-window at continuous sampling times, and the last sampling time is the current time. For example, at the sampling time t_j , the obtained raw data matrix $\mathbf{X}(t_j)$ is formed by

$$\mathbf{X}(t_j) = (\mathbf{x}(t_{j-T+1}), \mathbf{x}(t_{j-T+2}), \dots, \mathbf{x}(t_j)), \quad (15)$$

where $\mathbf{x}(t_k) = (x_1, x_2, \dots, x_t)^H$ for $t_{j-T+1} \leq t_k \leq t_j$ is the sampling data at time t_k . The fundamental abnormal detection and location procedures based on RMT is given as the steps below.

Fundamental Steps of RMT for Abnormal Detection and Location

- 1: Form a spatio-temporal dataset $\mathbf{D} \in \mathbb{C}^{p \times t}$ by arranging p observations in a series of time t .
- 2: At the sampling time t_j , obtain the raw data matrix $\mathbf{X}(t_j) \in \mathbb{R}^{P \times T}$ from the dataset \mathbf{D} .
- 3: Convert $\mathbf{X}(t_j)$ into the standard form matrix $\hat{\mathbf{X}}(t_j)$.
- 4: Calculate the sample covariance matrix $\Sigma(t_j) = \frac{1}{T} \hat{\mathbf{X}}(t_j) \hat{\mathbf{X}}(t_j)^H$.
- 5: Calculate the eigenvalues λ_{Σ} and the eigenvectors \mathbf{v}_{Σ} , and compare the empirical spectral distribution with their theoretical values.
- 6: Define and calculate the linear eigenvalue statistics $\mathcal{N}_{\Sigma}(\phi)(t_j)$ at the sampling time t_j .
- 7: Design an indicator $\eta(t_j)$ to measure the correlations between the outliers and the rows at the sampling time t_j , further determining the abnormal location.

III. INCIPIENT FAULT DETECTION AND LOCATION USING ONLINE MONITORING DATA

A. Formulation of Online Monitoring Data as Spatio-Temporal Matrices

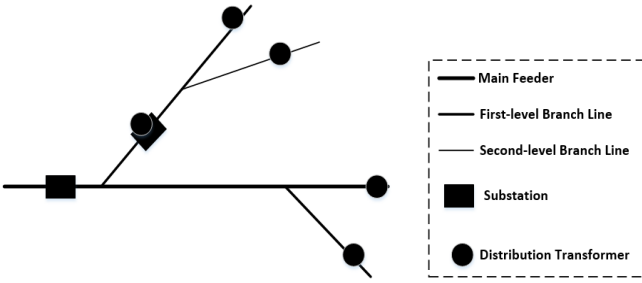


Fig. 3: Circuitry Topology of Distribution Networks.

Figure 3 illustrates circuitry topology of the distribution network. The main feeder consists of different levels of branch lines and substations with distribution transformers. On the low voltage side of each distribution transformer, one online monitoring device is installed, through which we can obtain many types of measurement variables such as three-phase voltages (i.e., u_a, u_b, u_c), three-phase currents (i.e., i_a, i_b, i_c), active load (l), etc. Running status of the main feeder can be reflected through those condition monitoring data. Here, we choose $u_a, u_b, u_c, i_a, i_b, i_c, l$ those 7 measurement variables

at the sampling time t_j as the elements to form a data vector $\mathbf{d}(t_j) = [u_{aj}^{(1)}, u_{bj}^{(1)}, u_{cj}^{(1)}, i_{aj}^{(1)}, i_{bj}^{(1)}, i_{cj}^{(1)}, l_j^{(1)}, \dots, l_j^{(m)}]^H$, where m denotes the number of distribution transformers on the main feeder. Assume $p = 7m$, for a series of time t , we can obtain a data matrix $\mathbf{D} = [\mathbf{d}(t_1), \mathbf{d}(t_2), \dots, \mathbf{d}(t_t)] \in \mathbb{R}^{p \times t}$. Since the measurements in \mathbf{D} have different units and magnitudes, we normalize \mathbf{D} into the matrix $\tilde{\mathbf{D}}$ by

$$\tilde{d}_{ij} = \frac{d_{ij} - \min(\mathbf{d}_i)}{\max(\mathbf{d}_i) - \min(\mathbf{d}_i)}, \quad (16)$$

where \tilde{d}_{ij} denotes the normalization value and $\mathbf{d}_i = (d_{i1}, d_{i2}, \dots, d_{it})$ for $i = 1, 2, \dots, p$ and $j = 1, 2, \dots, t$, $\min(\mathbf{d}_i)$ and $\max(\mathbf{d}_i)$ mean the minimum and maximum value in the i th row vector \mathbf{d}_i .

In order to amplify the sudden changes or the abnormal fluctuations of the observations for improving detection efficiency, we choose the residual matrix \mathbf{C} as our analyzing object, which can be obtained by

$$\mathbf{C} = \tilde{\mathbf{D}} - \hat{\tilde{\mathbf{D}}}, \quad (17)$$

where $\hat{\tilde{\mathbf{D}}}$ is the fitted matrix by using the autoregressive moving-average (ARMA) [21] model on $\tilde{\mathbf{D}}$, which is illustrated as

$$\hat{\tilde{d}}_{ij} = \begin{cases} \tilde{d}_{ij} & 1 \leq j \leq \alpha \\ \hat{\phi}_0 + \sum_{k=1}^{\alpha} \hat{\phi}_k \tilde{d}_{i(j-k)} + a_j - \sum_{l=1}^{\beta} \hat{\theta}_l a_{j-l} & \alpha < j \leq t \end{cases} \quad (18)$$

In equation (18), $\{(\hat{\phi}_k, \hat{\theta}_l)\}_{k \in [\alpha], l \in [\beta]}$ are the fitted model coefficients, $\{a_j\}$ is a white noise series, and (α, β) are the orders specified by the bayesian information criterion (BIC)[22][23].

Then we add white noise into the residual matrix \mathbf{C} to reduce the correlations among its rows. Let $\mathbf{E} \in \mathbb{R}^{p \times t}$ is a white noise matrix with standard normally distributed entries, the finally residual matrix with white noise is formulated by

$$\mathbf{X} = \mathbf{C} + \gamma \mathbf{E}, \quad (19)$$

where $\mathbf{X} \in \mathbb{R}^{p \times t}$ is the finally residual matrix and γ denotes the introduced white noise magnitude for the residual matrix \mathbf{C} . The signal-to-noise ratio (SNR) of the finally residual matrix \mathbf{X} is defined as

$$\tau_{SNR} = \frac{Tr(\mathbf{CC}^H)}{Tr(\mathbf{EE}^H) \times \gamma^2}, \quad (20)$$

where $Tr(\cdot)$ denotes the trace function of the matrix. In practice, the value of τ_{SNR} deserves carefully selected, which will affect the sensibility to the abnormal signal. Once the value of τ_{SNR} is set, γ can be calculated through

$$\gamma = \sqrt{\frac{Tr(\mathbf{CC}^H)}{Tr(\mathbf{EE}^H) \times \tau_{SNR}}}. \quad (21)$$

Thus, for each main feeder at the sampling time t_j , a finally spatio-temporal residual matrix \mathbf{X} is formulated.

B. Incipient Fault Detection and Location Method

Based on RMT and the formulated spatio-temporal residual matrices, an incipient fault detection and location algorithm in distribution networks is designed. The specific procedures are shown as follows.

Procedures of RMT for Incipient Fault Detection and Location

- 1: For each main feeder, form a spatio-temporal data matrix $\mathbf{D} \in \mathbb{R}^{p \times t}$ by arranging p observations in a series of time t .
- 2: At each sampling time t_j , construct the finally residual matrix $\mathbf{X}(t_j)$ by
 - a) normalizing $\mathbf{D}(t_j)$ into the matrix $\tilde{\mathbf{D}}(t_j)$ through equation (16),
 - b) calculating the fitted matrix $\hat{\mathbf{D}}(t_j)$ through equation (18),
 - c) formulating the residual matrix $\mathbf{C}(t_j)$ through equation (17),
 - d) introducing white noise into $\mathbf{C}(t_j)$, i.e. equation (19).
- 3: Convert $\mathbf{X}(t_j)$ into the standard form matrix $\hat{\mathbf{X}}(t_j)$ through equation (6).
- 4: Calculate the sample covariance matrix $\Sigma(t_j)$ through equation (7).
- 5: Calculate the eigenvalues λ_{Σ} and the eigenvectors \mathbf{v}_{Σ} of $\Sigma(t_j)$, and compare the empirical spectral distribution with their theoretical values.
- 6: Calculate the linear eigenvalue statistics $\mathcal{N}_{\Sigma}(\phi)(t_j)$ through equation (8).
- 7: Calculate the location indicator $\eta(t_j)$ through equation (14).
- 8: Draw the $\mathcal{N}_{\Sigma}(\phi) - t$ curve for each main feeder in a series time of t .

Procedure 1-3 are conducted for data preparing and preprocessing. In procedure 4-5, the ESD of the sample covariance matrix is computed and compared with their theoretical values, where MP-law and Ring-law are used as auxiliary analyzing tools. Procedure 6 and procedure 8, calculating the *LES* and drawing the *LES* – t curve, aim to detect the incipient faults. Procedure 7 calculates the location indicator, further locating the faults.

The incipient fault detection and location methodology proposed is driven by online monitoring data in distribution networks, and based on statistical theories. The procedures above involve no mechanism models, thus avoiding the errors brought by assumptions and simplifications. It merges fault detection and location functionalities, which makes it faster to detect and locate faults. Besides, the method is theoretically robust against random fluctuations and measuring errors, which can help to improve fault detection accuracy and reduce the potential false alarm probability. What's more, the proposed approach is practical for real-time fault detection and location by using the sliding-window method.

C. More Discussions about the Proposed Method

We may notice that the MP-law in the RMT holds under infinite or high data dimensions. However, in the application of incipient fault detection and location, there exist some main feeders with only a few distribution transformers. Dimensions of the formed data matrices corresponding to those main feeders are often moderate, such as tens or less. In , a natural way of increasing dimensions of data vectors is introduced. On this basis, here, we develop an approach to increase dimensions of data matrices. This approach allows for the analysis of high dimensional data matrices and yields smaller variance for the related functionals.

Assume $\mathbf{X} = [\mathbf{x}_1, \mathbf{x}_2, \dots, \mathbf{x}_t] \in \mathbb{C}^{p \times t}$ be a random matrix with i.i.d. entries, $p = kn$. For $k, t, n \in \mathbb{N}$, we construct a

new random vector by using the tensor product of the column vectors of \mathbf{X} in the form

$$\tilde{\mathbf{x}}_j = \mathbf{x}_j^{(1)} \otimes \dots \otimes \mathbf{x}_j^{(k)} \in (\mathbb{C}^n)^{\otimes k}, \quad (22)$$

where $\mathbf{x}_j^{(l)} (j = 1, 2, \dots, n; l = 1, 2, \dots, k)$ are i.i.d. copies of a normalized isotropic random vector $\mathbf{x}_j^{(1)} = (x_{1j}, \dots, x_{nj}) \in \mathbb{C}^n$ and ‘ \otimes ’ denotes tensor product operation. The new random vector $\tilde{\mathbf{x}}_j$ lies in the n^k dimensional normed space. Through the tensor product in equation (22), we obtain the dimension increased random matrix $\tilde{\mathbf{X}} = [\tilde{\mathbf{x}}_1, \tilde{\mathbf{x}}_2, \dots, \tilde{\mathbf{x}}_t] \in \mathbb{C}^{n^k \times t}$ regarding \mathbf{X} .

We consider $n^k \times n^k$ random matrices of the form[24]

$$\mathcal{M}_{n,t,k}(\mathbf{x}) = \sum_{\alpha=1}^t \tau_{\alpha} \tilde{\mathbf{x}}_{\alpha} \tilde{\mathbf{x}}_{\alpha}^H, \quad (23)$$

where $\tau_{\alpha} (\alpha = 1, 2, \dots, t)$ are real numbers. The asymptotic behavior of $\mathcal{M}_{n,t,k}(\mathbf{x})$ is well studied in [25]. For every fixed $k \geq 1$, as $t \rightarrow \infty, n \rightarrow \infty$, but $\frac{t}{n^k} \rightarrow c \in (0, \infty)$, the ESD of $\mathcal{M}_{n,t,k}(\mathbf{x})$ converges to a non-random measure.

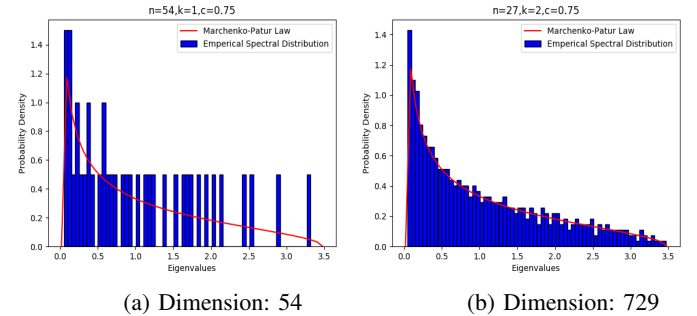


Fig. 4: ESD of $\mathcal{M}_{n,t,k}(\mathbf{x})$ and its comparison with the theoretical MP-law. The dimensions of data matrix \mathbf{X} is increased from $27 \times 2 = 54$ to $27^2 = 729$ through a tensor product of its column vectors, the radio c is 0.75, and τ_{α} is 1.

ESD of the original covariance matrix and the tensor product version and their comparisons with the theoretical MP-law are depicted in Figure 4a and Figure 4b respectively. It can be observed that the ESD of the original covariance matrix does not fit the theoretical MP-law for the reason of low dimensions of \mathbf{X} . In contrast, the ESD of the tensor product version of covariance matrix converges almost surely to the theoretical limit. This developed increasing data dimension approach makes it possible for the use of MP-law that require high dimensions as the prerequisite.

IV. CASE STUDIES

The methodology proposed in this paper is tested with both synthetic data from the standard IEEE bus system and real-world online monitoring data from a power grid. Five cases in different scenarios are designed to validate the effectiveness of the proposed method. In all the numerical cases, white noise is introduced to represent fluctuations and system errors.

A. Case Study with Synthetic Data

The synthetic data is sampled from the simulation results of the standard IEEE-118 and IEEE-30 bus system [26], with a sampling rate of 50 Hz. In the simulations, a sudden change of the active load at one node is considered as a signal.

1) Case Study on Effectiveness of Different Test Functions: In this case, the synthetic data set contains 118 voltage measurement variables with sampling 1000 times, size of the split-window is 118×200 , and τ_{SNR} is set to be 500. In order to test the effectiveness of the proposed method with different test functions, an assumed step signal is set for node 100 and others stay unchanged, which is shown in Table I.

TABLE I: ASSUMED SIGNALS FOR ACTIVE LOAD OF NODE 100 IN CASE 1.

Bus	Sampling Time	Active Power(MW)
100	$t_s = 1 \sim 500$	20
	$t_s = 501 \sim 1000$	100
Others	$t_s = 1 \sim 1000$	Unchanged

For comparing the effectiveness of the proposed method with different test functions, we normalize the calculated results into $[0, 1]$. The commonly used test functions are tested and Figure 5 illustrates the comparison results. It is noted that the $LES - t$ curve begins at $t_s = 200$, because the initial split-window includes 199 times of historical sampling and the present sampling data. Another needs to be noted is that the index number starts from 0 in Python.

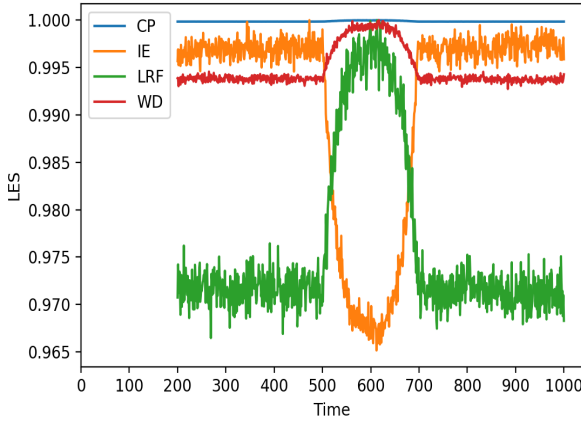


Fig. 5: Effectiveness of the proposed method with different test functions.

Based on the $LES - t$ curve, it can be observed that:

- During $t_s = 200 \sim 500$, LES computed through the proposed method with 4 different test functions remains almost constant, which means the system is under normal status. As is shown in Figure 6a and 6b, the ESD converges almost surely to its theoretical MP-law and Ring-law.
- From $t_s = 501$ to $t_s = 700$, LES changes dramatically, which means signal occurs and the system is under abnormal status. Figure 6c and 6d shows that there exist outliers.

III. At $t_s = 701$, LES recovers its initial value and remains almost constant afterwards, which means the system returns to normal status. Figure 6e and 6f shows that the outliers vanish and the ESD fits its MP-law and Ring-law again.

From the above analyses, we can conclude that the proposed method with any test function can detect the abnormal signal effectively and the delay lag of the signal to LES is equal to the split-window's width. More importantly, the $LES - t$ curve with test function IE has the highest variance radio, which indicates that it is more sensitive to abnormal detection than others. Therefore, we choose IE as the test function in the following cases.

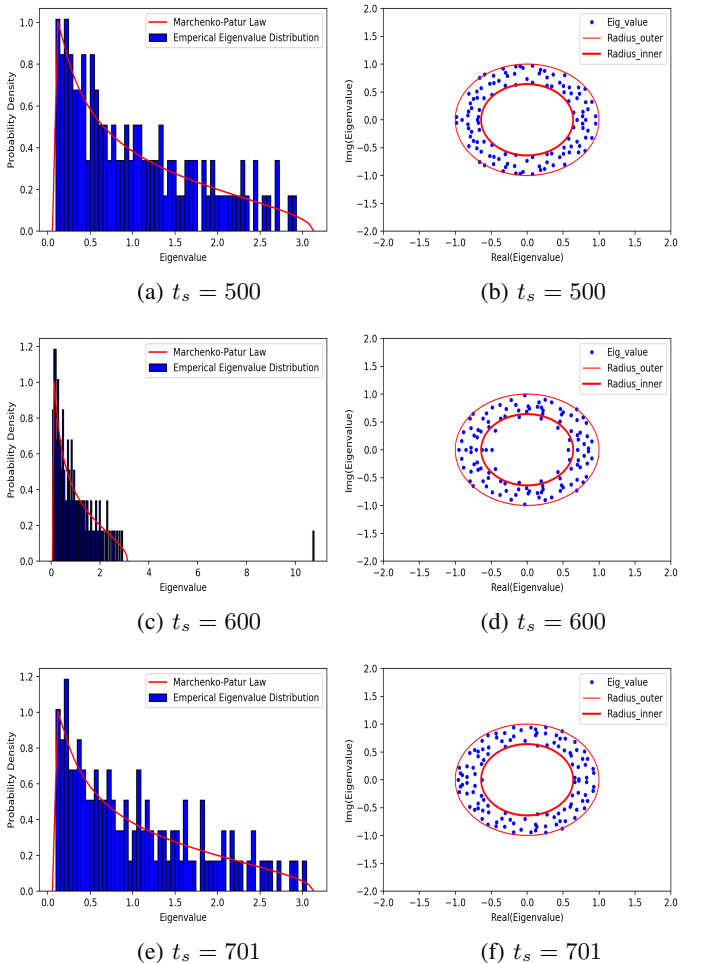


Fig. 6: ESD and its theoretical MP-law and Ring-law in case 1.

2) Case Study on Effectiveness of Increasing Data Dimension Method: In case 2, we aim to test the effectiveness of the proposed increasing data dimension method. The synthetic data from IEEE-30 bus system contains 30 voltage measurement variables, the split-window's size is 30×200 , the parameter τ_α is 1, and other parameters are set the same as in case 1. An assumed step signal is set for node 20 and others stay unchanged, which is shown in Table II. By using the proposed increasing data dimension method, dimensions of the matrices are increased from $30 = 15 \times 2$ to $225 = 15^2$.

The abnormal detection results are shown in Figure 7.

TABLE II: ASSUMED SIGNALS FOR ACTIVE LOAD OF NODE 20 IN CASE 2.

Bus	Sampling Time	Active Power(MW)
20	$t_s = 1 \sim 500$	20
	$t_s = 501 \sim 1000$	30
Others	$t_s = 1 \sim 1000$	Unchanged

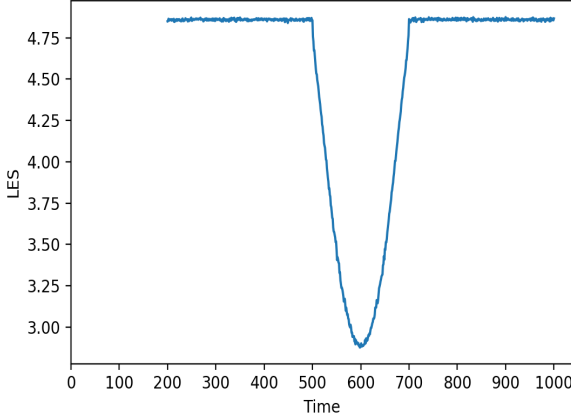


Fig. 7: Effectiveness of the proposed increasing data dimension method.

Based on the $LES - t$ curve, the assumed step signal for bus 20 can be detected below:

I. During $t_s = 200 \sim 500$, the value of LES remains almost constant, which indicates that the system is in normal state without signals. The ESD converges to its theoretical MP-law, which is shown in Figure 8a.

II. From $t_s = 501$ to $t_s = 700$, the $LES - t$ curve is almost U-shaped and the delay lag is equal to the split-window's width, which indicates that the signal occurs at $t_s = 501$ and remains afterwards. Besides, the $LES - t$ curve reaches its local minimum at $t_s = 600$, when just half of the split-window contains the signal. During this period of time, the ESD does not fit its theoretical MP-law, which is shown in Figure 8b.

III. At $t_s = 701$, LES increases back to its initial value and remains constant afterwards, which means the whole split-window contains the signal.

Analyses above are in accord with the assumed step signal in Table II. It indicates that the proposed increasing data dimension method is feasible for gaining high dimensional data matrices to meet the prerequisites for using RMT.

3) Case Study On Effectiveness of Abnormal Location Function: In case 3, the proposed abnormal location function both for high-dimensional and low-dimensional data matrices are tested.

3a) High-dimensional data scenario: The synthetic data set from simulation results of IEEE-118 bus system contains 118 active load measurement variables with sampling 1000 times. Parameters about the split-window are set the same as in case 1. Three assumed step signals are set for node 99 \sim 101, which is shown in Table III.

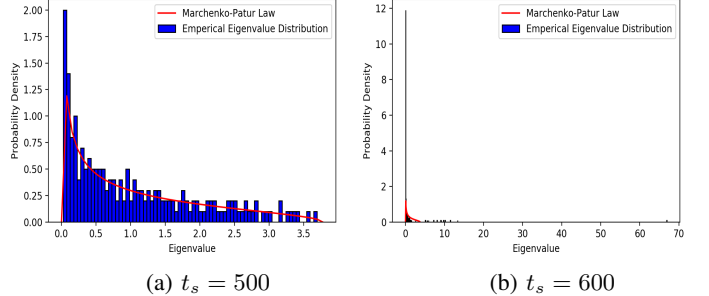


Fig. 8: The ESD and its theoretical MP-law in case 2: the data dimension is increased from $30 = 15 \times 2$ to $225 = 15^2$

TABLE III: ASSUMED SIGNALS FOR ACTIVE LOAD OF NODE 99 \sim 101 IN HIGH-DIMENSIONAL DATA SCENARIO.

Bus	Sampling Time	Active LOAD(MW)
99	$t_s = 1 \sim 500$	20
	$t_s = 501 \sim 1000$	80
100	$t_s = 1 \sim 500$	20
	$t_s = 501 \sim 1000$	100
101	$t_s = 1 \sim 500$	20
	$t_s = 501 \sim 1000$	120
Others	$t_s = 1 \sim 1000$	Unchanged

Figure 9 is the 3D plot of the location indicator η regarding IEEE 118 buses from $t_s = 200 \sim 1000$. It can be observed that:

I. During $t_s = 200$ and $t_s = 500$, no signal occurs and $\eta_i (i = 1, 2, \dots, 118)$ are small random real numbers nearly 0.

II. From $t_s = 501$, η_i corresponding to the nodes most affected by signals increase dramatically and reaches their peaks when half of the split-window contains those assumed signals, which are in accord with the signal detection processes. Thus, we can obtain the numbers of nodes (i.e., 99, 100, 101) with signals by getting those indexes corresponding to the η_i with obviously greater values.

3b) low dimensional-data scenario: In this scenario, the synthetic data set is the simulation results of IEEE-30 bus system and it contains 30 active load measurement variables with sampling 1000 times. Parameters of the split-window and others are set the same as in case 2. For each split-window, the dimension of data matrix is increased from 30 to 225 by using the proposed increasing data dimension method. Three assumed step signals are separately set for node 9 \sim 11 and node 19 \sim 21, which are shown in Table IV and Table V. The corresponding location results are shown in Figure 10a and 10b.

From the 3D plot Figure 10a of indicator η regarding IEEE-30 nodes and time, we can see that the values of η_i corresponding to indexes 121 \sim 165 are obviously greater than others from $t_s = 501$. Considering $n = 15$ in the increasing data dimension process, we can obtain the numbers of nodes (i.e., 9, 10, 11) with signals by getting round of those indexes divided by 15. In Figure 10b, it can be observed that η_i that

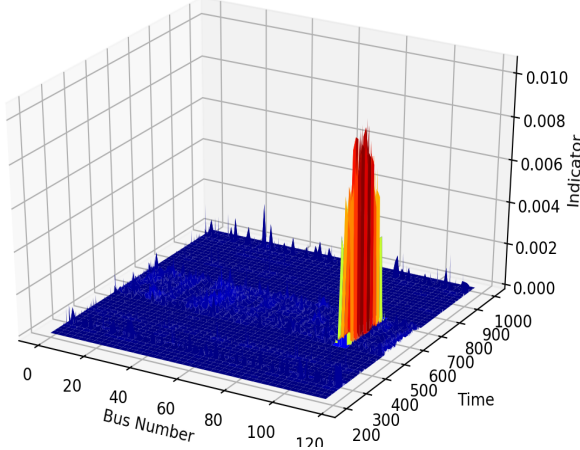


Fig. 9: Effectiveness of the proposed abnormal location function in high-dimensional data scenario.

TABLE IV: ASSUMED SIGNALS FOR ACTIVE LOAD OF NODE 9 ~ 11 IN LOW-DIMENSIONAL DATA SCENARIO.

Bus	Sampling Time	Active LOAD(MW)
9	$t_s = 1 \sim 500$	20
	$t_s = 501 \sim 1000$	80
10	$t_s = 1 \sim 500$	20
	$t_s = 501 \sim 1000$	100
11	$t_s = 1 \sim 500$	20
	$t_s = 501 \sim 1000$	120
Others	$t_s = 1 \sim 1000$	Unchanged

corresponds to indexes $4 \sim 6, 19 \sim 21, \dots, 214 \sim 216$ begin to increase at $t_s = 501$ and reaches their peaks at $t_s = 600$. combining the data division method in increasing data dimension process, we can locate the numbers of nodes (i.e., 19, 20, 21) with signals by getting sum of 15 with the mods of those indexes regarding 15.

Analyses of the proposed abnormal location function under both high-dimensional and low-dimensional data scenario indicate that it can effectively identify buses with signals. We will further test the location method in the following cases by using real-world online monitoring data in distribution networks.

B. Case Study with Real-World Online Monitoring Data

Online monitoring data obtained from a real-world distribution network are used to test the proposed incipient fault

TABLE V: ASSUMED SIGNALS FOR ACTIVE LOAD OF NODE 19 ~ 21 IN LOW-DIMENSIONAL DATA SCENARIO.

Bus	Sampling Time	Active LOAD(MW)
19	$t_s = 1 \sim 500$	20
	$t_s = 501 \sim 1000$	80
20	$t_s = 1 \sim 500$	20
	$t_s = 501 \sim 1000$	100
21	$t_s = 1 \sim 500$	20
	$t_s = 501 \sim 1000$	120
Others	$t_s = 1 \sim 1000$	Unchanged

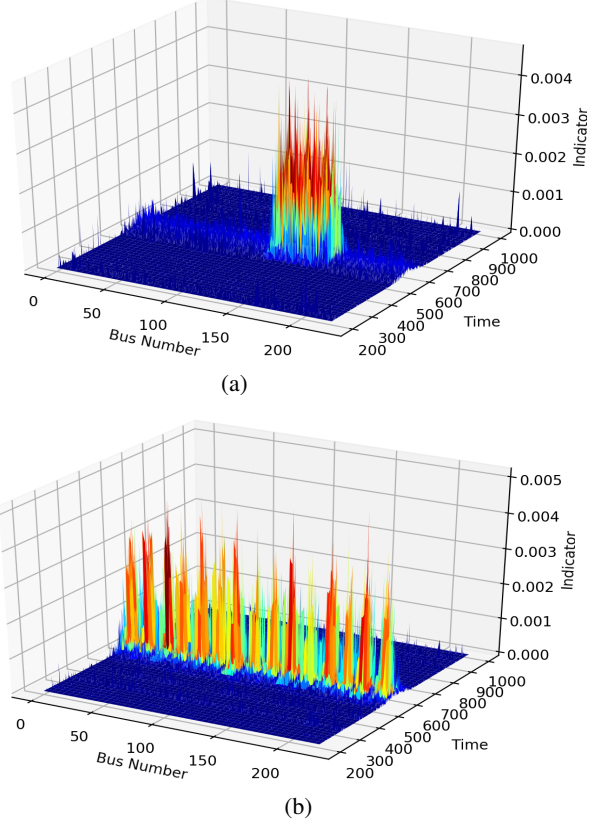


Fig. 10: Effectiveness of the proposed abnormal location function in low-dimensional data scenario.

detection and location method. The data is sampled every 15 minutes and the sampling time is from March 1st, 2017 to March 14th, 2017. Fault time and fault location for every main feeder are recorded. In the following cases, three-phase voltages, three-phase currents and active load measurements are chosen as the components to form the data matrix.

4) Case Study on High Dimensional Feeders: In case 4, the proposed method for high-dimensional feeder is tested. The selected main feeder with branch lines and substations contains 17 distribution transformers in total, thus forming a 119×1344 dataset. The size of the split-window is 119×192 , and the τ_{SNR} is set to be 100. The real-world online monitoring data with fault time and location recorded is shown in Figure 11. It can be obtained that the recorded fault time is 2017/3/8 13:47:00 and the fault induction are the branch lines or substations with ID 1554766408 and ID 1238878713 distribution transformers.

Figure 12 illustrates the detection results for the main feeder. From the $LES - t$ curve, we can realize the incipient fault detection as follows:

I. During 2017/3/3 00:00:00 and 2017/3/7 22:30:00, the value of LES changes smoothly, which indicates the main feeder runs in normal state.

II. At 2017/3/7 22:30:00, the value of LES begins to decrease dramatically. It indicates fault signals occur and the status of the main feeder change. According to the recorded fault time, the fault can be detected 15 hours and 17 minutes

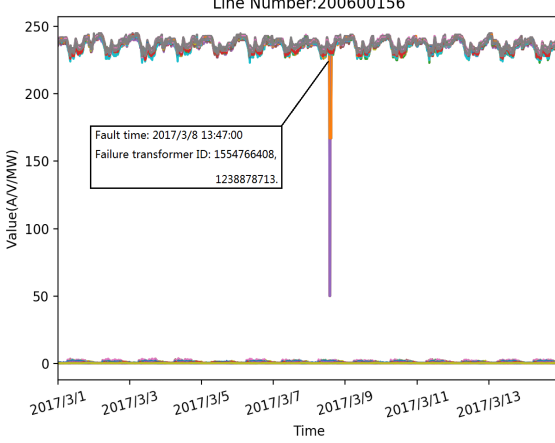


Fig. 11: Real-world data with fault time and location recorded in case 4.

before it happens. Meanwhile, from 2017/3/7 22:30:00 to 2017/3/9 23:45:00, the $LES - t$ curve is almost U-shaped and the delay lag is equal to the split-window's width, which is consistent with our simulation result in case 2.

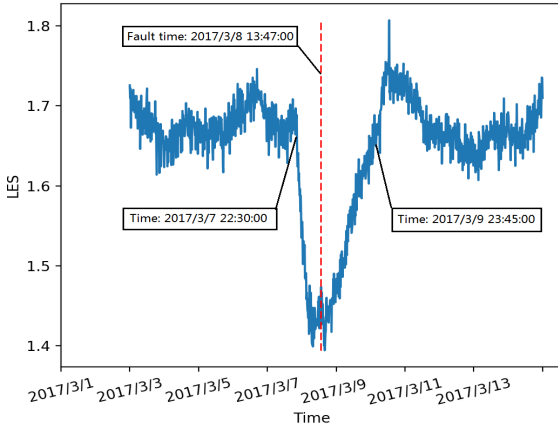


Fig. 12: $LES - t$ curve in case 4.

In real-time analysis, faults may happen any time after incipient fault signals occur and we may not observe the complete U-shaped curve. Therefore, the decreasing rate of LES for a series of time is usually calculated to judge whether incipient fault signals occur. Furthermore, by using the proposed fault location method, induction rows of data matrices are located, which is shown in Figure 13.

Figure 13 is the 3D plot of location indicator η regarding 119 observations from 2017/3/3 00:00:00 to 2017/3/14 23:59:59. At the incipient fault detection time, i.e., 2017/3/7 22:30:00, we obtain those indexes (i.e., 53, 54, 59, 60, 61) that correspond to the obviously larger calculated values of $\eta_i (i = 1, 2, \dots, 119)$. As 7 measurement variables for each distribution transformer are chosen to form the data matrix, we can locate fault transformers by getting round numbers of those obtained indexes divided by 7, i.e., NO.7 and NO.8

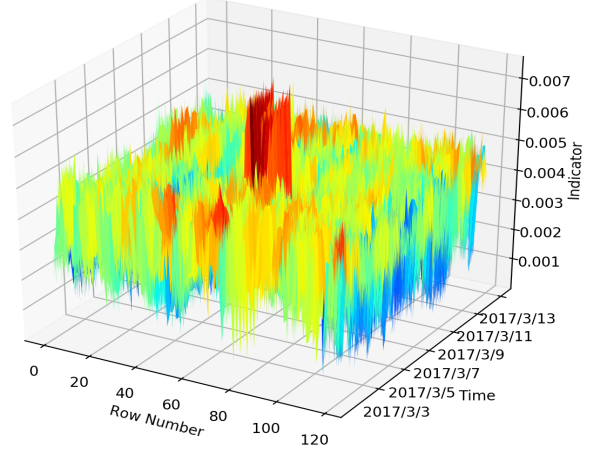


Fig. 13: Incipient fault location in case 4.

transformers. Transformer IDs that correspond to NO.7 and NO.8 are 1554766408 and 1238878713, which are in accord with the recorded failure transformer IDs. Thus, combining the topology of the main feeder, fault branch lines or substations with those 2 transformers can be identified and isolated in time.

5) Case Study on Low Dimensional Feeders: In this case, effectiveness of the proposed method for a low dimensional feeder is validated. We choose one main feeder with only 6 distribution transformers as our analyzing object. The size of the formed dataset is 42×1344 . The original online monitoring data with fault time and location recorded is shown in Figure 14. It can be seen that the recorded fault time are 2017/3/8 13:31:00 and 2017/3/13 03:10:00, and the failure transformer ID is 2513743732. By using the proposed increasing data

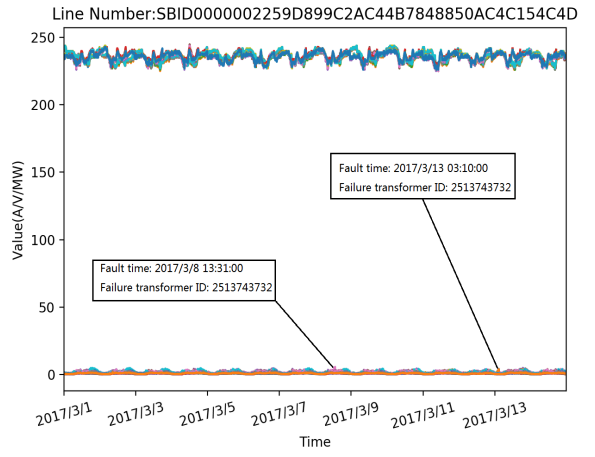


Fig. 14: Real-world data with fault time and location recorded in case 5.

dimension method, we increase the data's dimension from $42 = 21 \times 2$ to $21^2 = 441$. Thus, the size of the split-window is 441×192 and the SNR is set to be 100. The incipient fault detection result is shown in Figure 15.

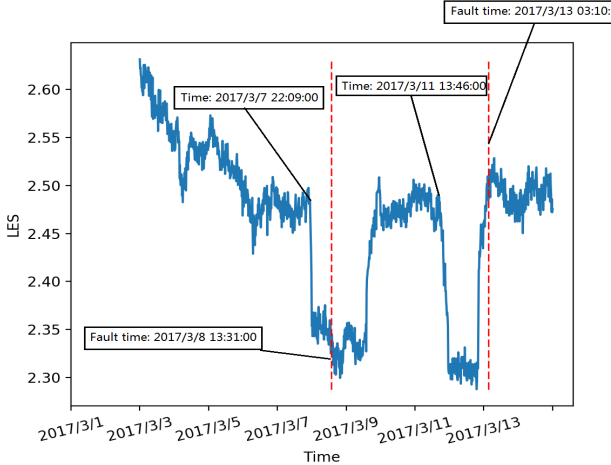


Fig. 15: $LES - t$ curve in case 5.

Based on the $LES - t$ curve, we can detect faults in an early phase as follows:

I. During 2017/3/3 00:00:00 and 2017/3/7 22:09:00, the value of LES changes smoothly, which means no fault signals occur and the status of the main feeder is normal.

II. At 2017/3/7 22:09:00, LES decreases dramatically, which indicates incipient fault signals occur and the status of the main feeder is getting worse. By comparing with the recorded fault time, we can detect faults 16 hours and 22 minutes before they happen. Besides, from 2017/3/7 22:09:00 to 2017/3/9 22:09:00, the $LES - t$ curve is almost U-shaped and the delay lag is equal to the split-window's width, which is consistent with our simulation results.

II. Similarly, at 2017/3/11 13:46:00, incipient fault signals are detected again 37 hours and 24 minutes before fault happens. It is noticed that the delay lag of the U-shaped $LES - t$ curve from 2017/3/11 13:46:00 to 2017/3/13 05:00:00 is not equal to the width of the split-window, which may be caused by the superposition of incipient fault signals with some other undesired signals.

Furthermore, we locate the faults by using the proposed location method, which is shown in Figure 16. From 2017/3/7 22:09:00, incipient fault signals occur and we obtain those $3 \times 21 = 63$ indexes (i.e., 1 ~ 63) that correspond to the top 63 calculated η_i ($i = 1, 2, \dots, 441$) in the dimension increased data matrix. Then we can get the corresponding row numbers (i.e., 1, 2, 3) in the original matrix through those indexes divided by 21. Considering 7 observations for each distribution transformer, we can locate fault transformers by getting round numbers of those obtained row numbers divided by 7, i.e., NO.0 transformer. Similarly, we can locate fault transformers at 2017/3/11 13:46:00. The obtained indexes are 1 ~ 42 and 106 ~ 126, and the calculated corresponding row numbers in the original data matrix are 1, 2 and 7, result of which divided by 7 is also NO.0 transformer. The ID corresponding to NO.0 transformer for this main feeder is 2513743732, which is in accord with the recorded failure transformer ID. Thus, we can identify the fault branch line or substation and isolate them before faults happen.

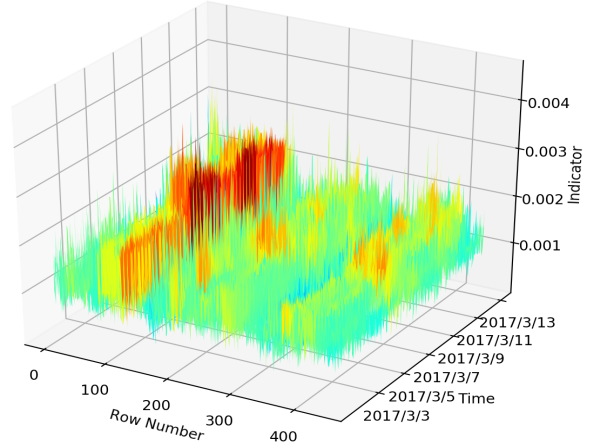


Fig. 16: Incipient fault location in case 5.

V. CONCLUSION

This paper develops a data-driven approach to realize incipient fault detection and location in distribution networks. For each main feeder, a spatio-temporal data matrix is formed as the data set by using online monitoring data of distribution transformers on it. The proposed methodology performs real-time fault detection and location by using a sliding-window method and the RMT, during which LES is calculated to indicate data behaviour and the MP-law and Ring-law are used as assisted tools to compare ESD and their theoretical findings. Meanwhile, for the data matrices formed by some low-dimensional main feeders, we develop an increasing data dimension method to meet the high dimension prerequisite for the use of RMT. As for the detected faulted feeders, analyzes of eigenvalues and eigenvectors corresponding to the outliers are conducted to locate the latencies. The proposed method is purely data-driven and it merges fault detection and location functionalities, which makes it suitable for real-time applications. Both synthetic and real-world data are used to corroborate the effectiveness of the proposed methodology and a software based it has been developed to put into practical application.

During our work, we notice that status of main feeders are directly related to the information of outliers, such as the number of outliers, the value of outliers, etc. Therefore, our future research could focus on the estimation methods of outliers and exploration of statistics regarding them.

REFERENCES

- [1] M. R. Jaafari Mousavi, "Underground distribution cable incipient fault diagnosis system," Ph.D. dissertation, Texas A&M University, 2007.
- [2] M. Pignati, L. Zanni, P. Romano, R. Cherkaoui, and M. Paolone, "Fault detection and faulted line identification in active distribution networks using synchrophasors-based real-time state estimation," *IEEE Transactions on Power Delivery*, vol. 32, no. 1, pp. 381–392, 2017.
- [3] L. Xie, Y. Chen, and P. R. Kumar, "Dimensionality reduction of synchrophasor data for early event detection: Linearized analysis," *IEEE Transactions on Power Systems*, vol. 29, no. 6, pp. 2784–2794, 2014.

[4] M. Wu and L. Xie, "Online detection of low-quality synchrophasor measurements: A data-driven approach," *IEEE Transactions on Power Systems*, vol. 32, no. 4, pp. 2817–2827, 2017.

[5] L. Chu, R. C. Qiu, X. He, Z. Ling, and Y. Liu, "Massive streaming pmu data modeling and analytics in smart grid state evaluation based on multiple high-dimensional covariance tests," *IEEE Transactions on Big Data*, vol. PP, no. 99, pp. 1–1, 2016.

[6] R. C. Qiu, Z. Hu, H. Li, and M. C. Wicks, *Cognitive radio communication and networking: Principles and practice*. John Wiley & Sons, 2012.

[7] N. A. S. B. K. Saad, *Random Matrix Theory with Applications in Statistics and Finance*. University of Ottawa (Canada), 2013.

[8] K. Chaitanya, "Random matrix theory approach to quantum mechanics," *arXiv preprint arXiv:1501.06665*, 2015.

[9] J. Watrous, "Theory of quantum information," *University of Waterloo Fall*, vol. 128, p. 19, 2011.

[10] X. He, Q. Ai, R. C. Qiu, W. Huang, L. Piao, and H. Liu, "A big data architecture design for smart grids based on random matrix theory," *IEEE transactions on smart Grid*, vol. 8, no. 2, pp. 674–686, 2017.

[11] X. Xu, X. He, Q. Ai, and R. C. Qiu, "A correlation analysis method for power systems based on random matrix theory," *IEEE Transactions on Smart Grid*, vol. 8, no. 4, pp. 1811–1820, 2017.

[12] W. Liu, D. Zhang, X. Wang, D. Liu, and X. Wu, "Power system transient stability analysis based on random matrix theory," *Proceedings of the CSEE*, vol. 36, no. 18, pp. 4854–4863, 2016.

[13] X. Wu, D. Zhang, D. Liu, W. Liu, and C. Deng, "A method for power system steady stability situation assessment based on random matrix theory," *Proceedings of the CSEE*, vol. 36, no. 20, pp. 5414–5420, 2016.

[14] R. C. Qiu and P. Antonik, *Smart Grid and Big Data: Theory and Practice*. Wiley Publishing, 2017.

[15] R. Qiu and M. Wicks, *Cognitive Networked Sensing and Big Data*. Springer Publishing Company, Incorporated, 2013.

[16] V. A. Marčenko and L. A. Pastur, "Distribution of eigenvalues for some sets of random matrices," *Mathematics of the USSR-Sbornik*, vol. 1, no. 4, p. 457, 1967.

[17] J. R. Ipsen and M. Kieburg, "Weak commutation relations and eigenvalue statistics for products of rectangular random matrices," *Physical Review E*, vol. 89, no. 3, p. 032106, 2014.

[18] A. Guionnet, M. Krishnapur, and O. Zeitouni, "The single ring theorem," *Annals of mathematics*, pp. 1189–1217, 2011.

[19] F. Benaych-Georges and J. Rochet, "Outliers in the single ring theorem," *Probability Theory and Related Fields*, vol. 165, no. 1-2, pp. 313–363, 2016.

[20] I. Jana, K. Saha, and A. Soshnikov, "Fluctuations of linear eigenvalue statistics of random band matrices," *Theory of Probability & Its Applications*, vol. 60, no. 3, pp. 407–443, 2016.

[21] G. E. Box, G. M. Jenkins, G. C. Reinsel, and G. M. Ljung, *Time series analysis: forecasting and control*. John Wiley & Sons, 2015.

[22] P. Stoica and Y. Selen, "Model-order selection: a review of information criterion rules," *IEEE Signal Processing Magazine*, vol. 21, no. 4, pp. 36–47, 2004.

[23] R. S. Tsay, *Analysis of financial time series*. John Wiley & Sons, 2005, vol. 543.

[24] A. Ambainis, A. W. Harrow, and M. B. Hastings, "Random tensor theory: Extending random matrix theory to mixtures of random product states," *Communications in Mathematical Physics*, vol. 310, no. 1, pp. 25–74, 2012.

[25] A. Lytova, "Central limit theorem for linear eigenvalue statistics for a tensor product version of sample covariance matrices," *Journal of Theoretical Probability*, pp. 1–34, 2017.

[26] R. D. Zimmerman, C. E. Murillo-Sánchez, and R. J. Thomas, "Matpower: Steady-state operations, planning, and analysis tools for power systems research and education," *IEEE Trans-* actions on Power Systems, vol. 26, no. 1, pp. 12–19, Feb 2011.